Correlated disorder in a *p*-wave superfluid

J. V. Porto* and J. M. Parpia
Laboratory of Atomic & Solid State Physics, Cornell University, Ithaca, New York 14853
(Received 20 November 1998)

The role of aerogel as a means of introducing correlated disorder into superfluid ^{3}He is examined in this paper. The aerogel structure is described by a diffusion-limited cluster aggregation model and compared to the results of small-angle x-ray scattering obtained from samples that were used to study the suppression of T_c as well as the development of the superfluid fraction. These results highlight special characteristics of aerogels that make this medium appropriate as a means of introducing disorder into ^{3}He. We discuss the inapplicability of the Abrikosov-Gorkov model of an impure superconductor to the ^{3}He-aerogel system, and then detail the behavior of T_c and the superfluid fraction of ^{3}He contained in three different samples of aerogel. [S0163-1829(99)03621-8]

I. INTRODUCTION

Over the last decade there has been increasing interest in the effects of impurities and disorder on phase transitions, particularly in unconventional superconductors. A number of experimental[1–6] and theoretical[7–9] investigations have followed the discovery of superfluidity of ^{3}He in aerogel which is the only system available for the study of disordered *p*-wave superfluids. Pure ^{3}He is an excellent starting point because it is extremely clean, its properties are well understood, and it does not need the extensive sample preparation required to examine the intrinsic properties of superconductors. In addition, the coherence length of ^{3}He can be changed simply by varying the pressure, allowing the relative strength of the impurity scattering to be easily altered without modifying the actual impurity density or correlations.

Surprisingly, the various experiments indicate that the suppression of the superfluid transition shows substantial variation even for ^{3}He which fills aerogels of very similar volume densities.[1–3,5,6] We present here evidence that the structural correlations within the aerogel (which directly affect the spatial correlations of the superfluid order parameter) are very important for determining the behavior of the transition temperature and superfluid density. To demonstrate this, we have performed small-angle x-ray scattering on two 98.2% open aerogel samples that we previously used for superfluid helium studies, but which exhibit quantitatively different phase diagrams.

We start by describing the structure of aerogels and examine a diffusion-limited cluster aggregation (DLCA) model that produces a realistic manifestation of a silica aerogel in the base catalyzed regime. We briefly present details of the construction of torsion pendulum oscillators used in this work and details of the small-angle x-ray measurements. Measurements of the structural correlations of the different aerogels are reported, and the results of the superfluid measurements are discussed in this context. We also discuss the scaling and temperature development of the superfluid fraction at different pressures with reference to recent theories.

II. AEROGEL STRUCTURE

Aerogels have almost all the properties required if one wishes to add impurities to ^{3}He. Aerogels are dilute, have a controllable density, and are easily introduced into liquid ^{3}He, which has no other source of impurities. In addition, the correlations between the silica clusters can be altered by adjusting the growth chemistry. It must be fully appreciated, however, that aerogel is by no means random and there are always strong structural correlations present within it. We note that these correlations are completely unavoidable: since low-temperature ^{3}He is a completely immiscible liquid, any low density ''impurity'' must be able to rigidly support itself, and will necessarily have structural correlations. In addition, these correlations will extend over longer and longer length scales as the impurity is made more and more dilute. The purpose of this section is to describe the structure of aerogel and relate it to the behavior of ^{3}He contained within it.

The production and understanding of aerogels has advanced significantly in the last decade.[10] They can be easily made with a wide range of densities, and the resulting structure is well understood. The standard technique for making aerogel involves two essential steps: gelation of SiO_2 from solution and removal of the solvent after gelation. The properties of aerogels are largely controlled by the kinetic dynamics of the gelation process. Different growth dynamics can lead to different structure. The *p*H of the initial solution, for example, strongly influences the precipitation rate of the silica from solution.[11] For base catalyzed aerogels small silica particles precipitate very quickly, and the subsequent coalescing process of the silica into a gel is diffusion limited.[12,13] For neutrally reacted aerogels, the precipitation is slow, and the gelation is chemically limited. This is an important point, since structurally different aerogels of identical densities can be made by altering the gelation conditions. On the other hand, the volume densities can be accurately predetermined by carefully controlling the concentration of the initial solution. The aerogels used in this study were all grown in the base catalyzed regime,[14] and each had volume concentrations of 1.8% (98.2% open).

For base catalyzed aerogel, a structural picture has emerged from a variety of small-angle scattering[11,12,15] experiments. Small particles of SiO_2 with diameters $a \simeq 30$ Å coalesce into a fractally correlated structure. The fractal correlations extend up to a correlation length ξ_a, which is concentration dependent and is on the order of several hundred

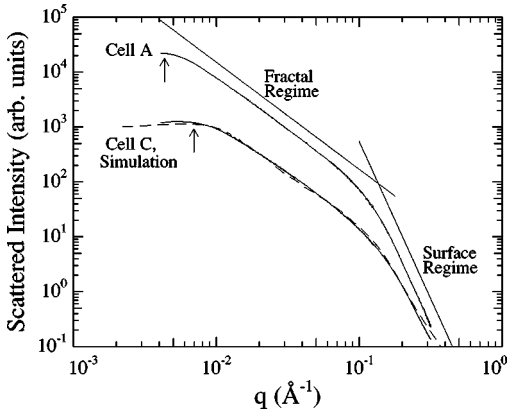

FIG. 1. Small-angle x-ray scattering from two different aerogels. The upper solid curve is for the aerogel sample from cell A and the lower solid curve is for the aerogel from cell C. (Both samples were 98.2% open). The dashed line is the scattered intensity calculated for the DLCA model aerogel described in the text. The homogeneous regime applies at small q, and is separated from the fractal regime (as indicated with the arrows) at $q \simeq 2\pi/\xi_a$. The fractal regime is separated from the surface regime at $q \simeq 2\pi/a$.

to a few thousand Å. The ''fractal'' dimension for these base catalyzed aerogels is usually found to be about 1.8, but the fractal regime barely extends over a decade for all but the most dilute samples. Above the length scale ξ_a, the system looks homogeneous. Below the length scale a, the scattered intensity arises predominantly from the surface of the particles, which themselves can have fractallike properties. These features are illustrated in Fig. 1, where we have plotted the scattered intensity from two different aerogels. The correlations in the fractal and surface regimes can be determined by measuring the power-law behavior of the scattering in those regimes. The aerogel structure can therefore be described by four parameters determined from small-angle scattering. The two length scales ξ_a and a divide the scattering into three regimes: a homogeneous, fractal, and surface regime. The slopes in the fractal and surface regimes, K_f and K_s, determine the nature of the correlations at those length scales. In addition, the volume concentration c gives the average density of SiO_2, and is the fifth parameter that can be used to characterize the aerogel. It is evident that by itself, c is inadequate to fully describe aerogel and therefore its effect on the properties of superfluid ^{3}He.

The picture is different for neutrally reacted aerogels. In this case there is no smallest unit particle, and the structure can be fractally correlated down to almost atomic length scales.[11] The fractal dimension is significantly larger,[11] $\simeq 2.4$, and the correlation length ξ_a is larger than for base catalyzed gels of the same density. For neutrally reacted aerogels therefore the fractal regime can extend over two decades of length. There are some experimental drawbacks to using neutrally reacted aerogels, however. They gel very slowly (in fact may not gel at all at low enough densities[16,17]), and they may tend to have a few very large open pores.[17]

For both growth environments, it is clear that aerogel is not a ''porous'' medium in the strictest sense, since there are no conventional pores with well defined walls. In fact, if we take the superfluid coherence length ξ_0 as the appropriate length over which the superfluid samples its environment, there aren't any real ''surfaces'' within aerogel at all, since $\xi_0(\simeq 150\text{–}800\ \text{Å}) > a(\simeq 30\ \text{Å})$. At the atomic length scale, though, aerogel does have an enormous surface area, which has been measured in one of our samples to be about 25 m^2/cm^3 using ^{3}He vapor pressure isotherms.[18] This surface area has been shown[4,5] to have important implications for the behavior of the superfluid since the liquid is in fast exchange with the polarizable solidlike surface layer of ^{3}He.

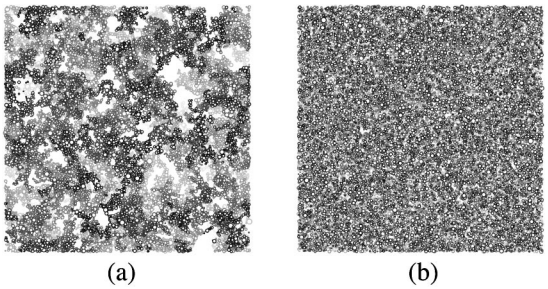

FIG. 2. Panel (a) shows the projection of a cube of aerogel, $\simeq 3500$ Å on a side, simulated with the DLCA model. The aerogel has a volume concentration of 0.018 (98.2% open). The particle diameters have a Gaussian distribution around $\simeq 30$ Å, with width $\sigma = 15$ Å. The particles are plotted on a gray scale according to their z position, with the darkest in the foreground. For comparison we show in panel (b) a 3500-Å cube containing a random arrangement of spheres with the same diameters and volume fraction as the aerogel cube shown in (a).

In addition to the k-space information available from small-angle scattering measurements, accurate models of aerogel formation can provide a good real-space picture of the structure. For base catalyzed aerogels which are in the diffusion-limited growth regime, the DLCA model[13,15,19,20] provides an extremely good representation of aerogel. We have implemented a version of the model described by Hasmy and co-workers[13,15] to simulate the structure of the aerogels used in our experiments. The scattering intensity calculated from the model structure is also shown in Fig. 1 along with the actual scattered intensities. There are two fit parameters which set the intensity and overall length scale. Since these parameters set overall scales, on a log-log plot they correspond merely to shifting the scattering curve up/down and left/right, respectively, with no alteration of the shape of the curve. A third, less critical fit parameter is the degree of polydispersity of the constituent particles which affects only the short distance, high q part of the structure. The agreement for one of the aerogels is good over the length scales shown, and implies that for that aerogel, the simulation accurately represents the structure between $\simeq 20$ and $\simeq 2500$ Å. Above 2500 Å we expect the structure to be essentially homogeneous for base catalyzed aerogels.[13]

Figure 2(a) shows a numerically simulated cube of 98.2% open aerogel, 3500 Å on a side. This representation of a three dimensional solid projected onto two dimensions is intended to replicate the view observed in a TEM image. For comparison, we show in Fig. 2(b) a cube of randomly placed spheres of the same volume density. These images are somewhat misleading since all the silica in the entire depth of the aerogel cube has been projected onto the page. A 300 Å slice of the simulated aerogel is shown in Fig. 3(a) in order to

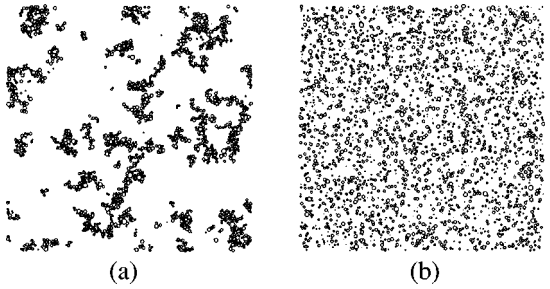

FIG. 3. Panel (a) shows a 300-Å-thick slice of the aerogel shown in Fig. 2(a). A similar slice of the random arrangement of spheres is shown in panel (b).

adequately illustrate how dilute the structure is. The structure is clearly correlated on this length scale, and for comparison, a similar slice of randomly placed silica is also shown in Fig. 3(b).

With an accurate real-space model in hand, we can now address questions about relevant length scales. A natural question arises: What is the fraction of the volume that is farther than a distance x from the SiO_2? Figure 4 shows the distribution $P(x)$ of nearest distances x to SiO_2 for the model 98.2% aerogel. It was generated by picking random points within the cube of aerogel, and then calculating the nearest distance to any SiO_2 particle. The plot is the normalized histogram of these distances. Integrating this curve gives the probability of being closer than x to SiO_2, which is also shown in Fig. 4. Despite the fact that aerogel is so dilute, we find that *all of the volume is within 350 Å of some* SiO_2. One consequence of this efficiently distributed yet highly open structure is that the probability of being closer than x to aerogel changes rapidly over a very short distance: half of the volume is farther than 100 Å from silica, but none of it is farther than 350 Å. The coherence length of ^{3}He ranges between $\simeq$150 Å at high pressure to near $\simeq$800 Å at low pressure. The absence of larger than 350 Å cavities implies that essentially all the Cooper pairs (which have size $\geqslant \xi_0$) will encompass one or more of the silica aggregates. Consequently, it is correct to conclude that the silica, on average, penetrates to the interior of the Cooper pairs. The distribution of silica shown in Fig. 4 is particularly well matched to

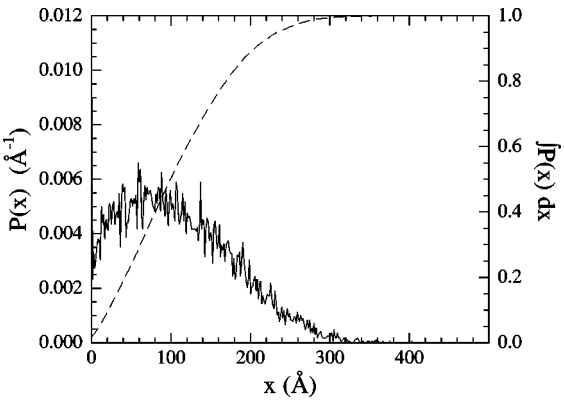

FIG. 4. The solid line represents the distribution $P(x)$ of nearest SiO_2 distances within the open volume of the simulated aerogel. $P(x)dx$ is the probability that a randomly chosen point within the aerogel is a distance $x \pm dx/2$ from SiO_2. The dashed line represents the integral of $P(x)$.

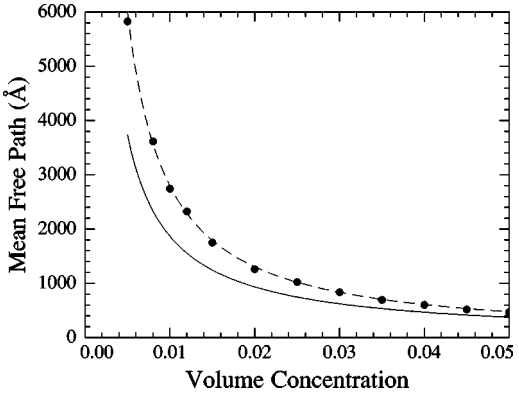

FIG. 5. The geometrical mean free path l_g for simulated aerogel as a function of volume concentration. The solid line is the geometrical mean free path for a random distribution of particles of the same diameter. The dashed line was determined from a fit to a power law, and is given by the equation $l_g = 17.6c^{-1.1}$ Å.

the pressure dependence of ξ_0, since even at high pressure most of the pairs will interact with the silica, and at low pressure the coherence length spans the entire distribution of correlation lengths in the aerogel.

The fractal correlations on length scales between a and ξ_a have physical significance for straight line trajectories (for example of a quasiparticle) within the aerogel. The ability of a trajectory to traverse a fractal object depends on the object's fractal dimension D. For objects in three dimensions, the codimension $(3-D)$ is a measure of the object's ''openness'' to straight-line trajectories.[21] For true fractals, if $(3-D)>1$, a random line will not intersect the object, and if $(3-D)<1$, a random line will intersect the object. As discussed above, base catalyzed aerogels usually have a ''fractal'' dimension between 1.7 and 1.9, so that the codimension $(3-D)$ is larger than 1. This indicates that the structure is less likely to obstruct straight-line trajectories, and thus longer mean free paths should be observed in these aerogels. We stress that this statement can be made only in a very approximate sense, because the fractal correlations are present over such a narrow range of lengths. For neutrally reacted aerogels, the fractal correlations extend over a much larger range, and the dimension can be as high[11] as 2.4, indicating that the structure is *not* very open to straight-line trajectories. (That two objects of the same average density can have different mean free paths is not surprising. A soap bubble foam and a jungle gym, for example, can be arranged to have similar average densities, but drastically different mean free paths.) This observation could have significant implications for studies of ^{3}He in aerogel because it should be possible to grow aerogels with identical densities, but with different mean free paths.

The enhancement of the mean free path (compared to that of a random arrangement of spheres) is shown for the simulated aerogel in Fig. 5. We plot the geometric mean free path l_g, calculated directly from the model aerogel as a function of volume concentration, and the equivalent mean free path for a random arrangement of spheres given by $l_{rand} = \frac{2}{3}ac^{-1}$, where a is the diameter of the constituent spheres. The aerogel mean free path is somewhat larger than for an uncorrelated system (as expected from the arguments presented above), and we find that below 5%, l_g scales as $c^{-1.1}$.

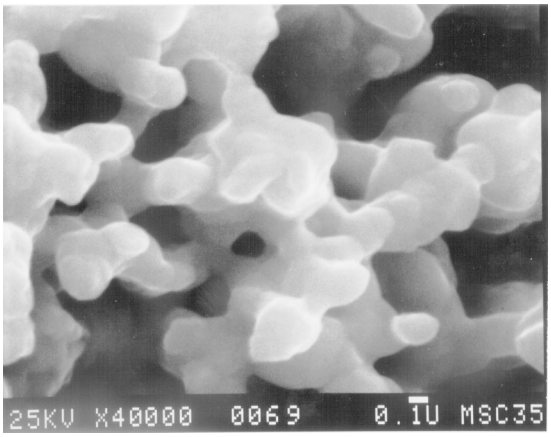

FIG. 6. A scanning electron microscopy picture of a 50% sinter, made from 800-Å nominal diameter silver powder. Compare the length scale to the size of the aerogel in Fig. 2. Almost the entire cube shown in Fig. 2 can fit inside a single pore of the sinter.

For a 95% aerogel $l_g = 500$ Å, but it grows to 1800 Å for a 98.5% aerogel. A 99% aerogel would have a mean free path of almost 3000 Å. Since the mean free path of bulk ^{3}He quasiparticles diverges at low temperature as $1/T^2$ (at 2 mK and low pressures, for example, it is already larger than 10 μm) the quasiparticle scattering will be dominated by the aerogel. The aerogel limited mean free path will certainly depend in detail on the scattering of quasiparticles from the aerogel surface. In particular, the nature of that scattering, whether elastic or inelastic, is probably affected[4] by the surface layers of ^{3}He. It is evident, however, that the upper limit of the quasiparticle mean free path will be set by the geometric mean free path determined by the aerogel.

From the discussion in this section, it is evident that aerogels have a unique structure distinguished from those of other porous media. The small scale of the silica allows the aerogel to function as an impurity, and almost all of the volume is within a superfluid coherence length of some SiO_2. For comparison, in Fig. 6 we show a SEM picture of a 50% packed silver sinter which gave a similar superfluid fraction as the aerogel samples.[22] We note that almost the entire 3500 Å cube of aerogel shown in Fig. 2(a) can be fit inside any of the pores of this silver sinter. It is thus clear that the structure of aerogel is uniquely suited to the study of impurity effects on superfluid ^{3}He.

III. EXPERIMENTAL DETAILS

A. Cell design

We examined ^{3}He superfluid in three different aerogel samples using the standard torsion pendulum technique.[23] Since the normal-fluid viscous penetration depth exceeds the aerogel strand separation by several orders of magnitude, the normal fluid contributes its entire moment of inertia to the torsional pendulum. The superfluid component also contributes to the moment of inertia due to geometry dependent nonviscous forces, but since the aerogel is so open this contribution is rather small. We have measured the fraction of superfluid coupled to the oscillator χ to be 0.05 using superfluid ^{4}He. The superfluid density is therefore directly proportional to the period shift $\Delta P(T)$ through the equation

$$\rho_s/\rho = \frac{1}{1-\chi}\frac{\Delta P(T)}{\Delta P_{fill}}. \quad (1)$$

The sensitivity of the oscillator is calibrated using the period shift upon filling the cell with ^{3}He, ΔP_{fill}. In practice, the analysis can be complicated by gaps between the aerogel and the cell walls which are filled with bulk fluid, but the behavior of bulk ^{3}He is sufficiently well known that these effects can be accounted for.

The first two cells, A and B, were of almost identical design and were studied on a $PrNi_5$ nuclear demagnetization cryostat. The body of the torsional oscillators were made of beryllium copper, and the silver sinter heat exchangers were of standard design. Cell C was intended for use at very low temperatures on a copper demagnetization stage. The body of the oscillator was made of coin silver, and a pure silver rod was used to thermally link the silver sinter heat exchanger to the demagnetization stage. A small secondary heat exchanger was located to intercept any residual heat load coming down the fill line. For all three cells the thermal lag was found to be no more than 10 μK at the warming rates used in temperature sweeps (on the order of 25 μK/hr). The cells were operated at their resonant frequency using a circuit that maintained a constant amplitude of motion. In the experiments described here, all heating due to internal dissipation was found to be insignificant at the amplitudes that were used.

The samples were grown for us at Penn State directly into metal cups.[14] For cells A and B, the cups were stainless steel, and in cell C the cup was pure silver. These cups were then epoxied into a mating cup in the respective torsional oscillators. In cell A the aerogel completely filled the cell and there was no contribution to the period shift from the bulk fluid. For sample B, the cup had a concentric cylindrical plate capacitor fabricated from a stainless steel mesh. This capacitor allowed the *in situ* determination of the ^{3}He/^{4}He ratio within the aerogel. Its use will not be discussed in much detail, because the presence of this device led to the generation of numerous internal resonances in the superfluid state which obscured the temperature dependence of the superfluid fraction.

In cells B and C there was a small gap which contributed a bulk ^{3}He signal to the period shift. As discussed above, the bulk fluid properties are sufficiently well known that the bulk contribution to the period shift can be accounted for. For example, Fig. 7 shows the unadjusted period of cell C at 20 bar, along with the properly scaled temperature dependence of the bulk superfluid.[24] In cell B, the bulk gap was large enough that the viscosity of the bulk fluid must also be taken into account.[25] An example of the bulk contribution to cell B's period and the scaled behavior of bulk ^{3}He are shown in Fig. 8. For both cells the bulk contribution was subtracted from the total period shift to yield the superfluid fraction.

B. X-ray scattering

The aerogel samples were carefully removed from the torsional oscillators and were machined to reduce the sample from an initial thickness of 8 mm down to a final thickness of 1 mm. Small-angle x-ray scattering on these samples was performed at the Cornell High Energy Synchrotron Source

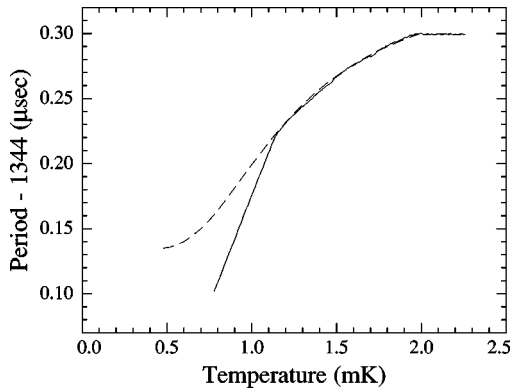

FIG. 7. The period as a function of temperature for ^{3}He at 13.7 bar in cell C. The scaled bulk contribution[24] is indicated by the dashed line.

with the help of Ernie Fontes and Lois Pollack. The experiment was carried out at the D station, which is a bending magnet line with a double bounce multilayer monochromator. The monochromator was set to operate at 1.54 Å, the beam was collimated to 0.3×0.3 mm and we used a 1024×1024 charge-coupled device area detector with a pixel spacing of 50.8 μm. The measurements taken at the smallest angles were made with a sample to detector distance of 1.3 m.

IV. RESULTS

Superfluid ^{3}He has been studied in several different aerogel samples to date.[1–6] The superfluid transition temperatures in aerogel, T_c^a, measured in cells A, B, and C are shown in Fig. 9, along with the results for two other samples measured at Northwestern[2] and Manchester.[5] While there is reasonable agreement between samples B, C, and the results obtained at Northwestern, it is clear that there are substantial differences between these and the results of sample A, while the Manchester T_c^a data are intermediate. All five samples had a nominal aerogel volume fraction of $\sim$1.8%, and the quantitative differences clearly indicate that some other property of the aerogel, presumably structural correlations, plays an important role. In addition to the differences in transition temperatures for the various samples, the behavior of the superfluid density is qualitatively quite different from bulk ^{3}He, and also for that calculated for ^{3}He containing homogeneously scattering impurities. In this section we discuss measurements of the structural correlations for two of our aerogels (samples A and C) and discuss the consequences of the structural differences for the behavior of the superfluid. Since the variation of the superfluid transition temperatures recorded for these two samples represent the extreme values for this (98.2% open) aerogel density, such a comparison has important implications for sample preparation in the future, and for the understanding of the effect that the structural correlations have on T_c^a. We will also describe scaling properties of the superfluid density which point to a qualitative as well as quantitative disagreement with a model based on the Abrikosov-Gorkov theory of suppression of T_c by scattering.

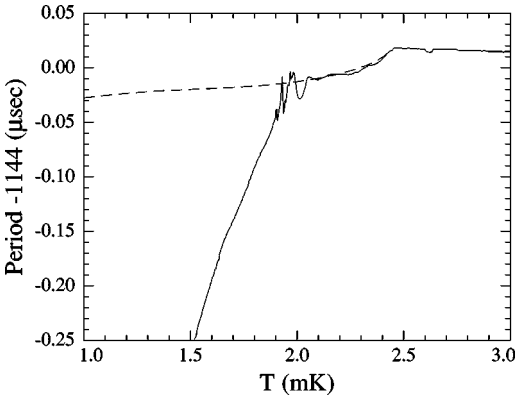

FIG. 8. The period as a function of temperature for ^{3}He at 29.7 bar in cell B. The scaled bulk contribution is indicated by the dashed line. Due to the size of the gap containing bulk fluid, the bulk signal is not merely proportional to the bulk superfluid density and the viscosity of the normal fluid fraction must also be taken into account. Resonances near T_c^a make the identification of the transition temperature difficult.

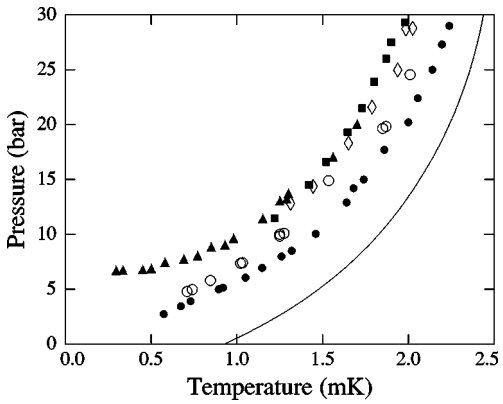

FIG. 9. Transition temperatures T_c^a as a function of ^{3}He pressure. The solid line is the bulk transition temperature dependence due to Greywall (Ref. 26). The solid circles, squares, and triangles are from cells A, B, and C, respectively. The open diamonds are the results from Northwestern (Ref. 2) and the open circles are the results from Manchester (Ref. 5).

A. Results of small-angle x-ray scattering

The manifestation of structural differences in samples A and C can be seen in Fig. 1. (Since the transition temperatures measured in sample B are very similar to those in sample C, we assume that the structure is also very similar.) There are clear differences in almost all of the characteristic properties of the two samples. All of the four parameters, ξ_a, a, K_f, and K_s (described in Sec. II), are different for the two samples. The aerogel in cell A was one of the very first samples made for us by Moses Chan's group. Unfortunately, at that time we were unaware that any characteristic of the aerogel other than density was significant. Consequently, the mass concentration was carefully determined, but the gelling conditions for the first cell were not documented. The early cells were typically gelled more slowly than the later ones, and we speculate that sample A was catalyzed in a less basic environment than sample C.

The DLCA model accurately describes sample C, and a good estimate of a can be made by fitting the scattering from the model aerogel to the experimental scattering data. We

TABLE I. Values of the five structural parameters discussed in the text for cells A and C.

	ξ_a (Å)	a (Å)	K_f	K_s	c
Cell A	1300	$\simeq 30$	-1.91	-5.7	0.018
Cell C	840	28	-1.83	-4.5	0.018

obtain an average particle diameter $a \simeq 28$ Å for sample C. Without a model for the aerogel in sample A it is more difficult to accurately establish a length scale, but by comparing the two scattering plots we estimate the average particle size in sample A to be about 10% larger than in sample C.[27] All five parameters for the two cells are summarized in Table I.

At the smallest length scale the slopes of the surface scattering regime K_s are slightly different. While a slope of $K_s = -4$ would indicate scattering from smooth surfaces, we find $K_s = -5.7$ for sample A and $K_s = -4.5$ for sample C, indicating that the constituent particles have rough, correlated surfaces. The difference in the slopes points to possible differences in the microscopic surface area of the two aerogels, but unfortunately we measured the surface area of only one of the samples.[1] While it has been shown that surface ^{3}He can have a significant effect on the internal structure of the superfluid,[4,6] we have found[28] that replacing the surface ^{3}He with ^{4}He has only a small effect on the measured ρ_s and T_c^a. We therefore believe that disparities in the surface structure are *not* the origin of the different results obtained with different aerogels.

The largest difference is in the correlation length ξ_a, where we find $\xi_a \simeq 1300$ Å for sample A and $\xi_a \simeq 840$ Å for sample C. The slopes in the ''fractal'' regime also differ slightly, although it is difficult to define a slope for sample C because the fractal regime extends over such a limited range. Given that the two ξ_a differ, we expect the fractal correlations to be different, since for aerogels of identical density the three parameters ξ_a, K_s, and K_f are not independent.[11] We find $K_f = -1.9$ in sample A and $K_f = -1.8$ in sample C. While the fractal nature of the impurity density may play a role in the behavior of the superfluid, it occurs mostly on a length scale smaller than the coherence length. The significant difference in ξ_a between the two samples is likely to strongly affect the superfluid. These differences help explain the differences in T_c, and as we will discuss below, it also helps understand the behavior of the superfluid density as a function of temperature and pressure.

B. Breakdown of the Abrikosov-Gorkov model

One of the most exciting aspects of the discovery of superfluid ^{3}He in aerogel was the extreme sharpness of the superfluid transition.[1] In NMR studies[2] this was particularly important since NMR is a local probe of the superfluid order parameter, and the sharpness of the transition indicates a global transition. At present there is no conclusive evidence which rules out the possibility of local regions of superfluid with transition temperatures between the bulk T_c and the suppressed T_c^a. Experiments at Manchester show that simultaneous NMR and torsion pendulum results reveal identical T_c^a, but it is possible that (depending on the l texture orientation) a positive frequency shift from one region may be canceled by a negative shift from another region for $T_c^a < T < T_c$. Results from Stanford[6] indicate that superfluid textures are sensitive to inhomogeneities within the aerogel. We note however, that while aerogel has significant structure at the same length scale as the order parameter, above this length it can be quite homogeneous. In this light the superfluid transition should be global, even if the local order parameter is finite above T_c^a for small regions on the order of the coherence length. This situation would be analogous to Josephson coupled superconducting grains in a thin film. Heat-capacity measurements underway should be able to provide a definitive answer for whether there is a local superfluidity that precedes the onset observed in these experiments and with NMR.

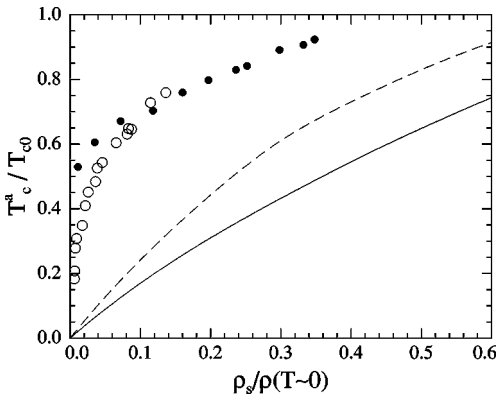

FIG. 10. The aerogel suppressed transition temperatures T_c^a normalized to the bulk transition temperatures T_c^0 as a function of low-temperature superfluid fraction. The filled circles are for the data from cell A and the open circles are for the data from cell C. The two lines are results from Hanninen *et al.* (Ref. 33) based on the Abrikosov-Gorkov model for homogeneously scattering impurities in superfluid ^{3}He. The dashed curve is the result in the unitary limit. [It has been shown (Refs. 7 and 33) that the unitary limit represents the upper limit of T_c/T_{c0} at a given ρ_s/ρ.] The solid curve is the result halfway between the Born and unitary limits, which is most likely to be appropriate for ^{3}He in aerogel (Ref. 33).

These results, and the small size of the aerogel particles (relative to ξ_0) suggested that for the first time impurities had been introduced into superfluid ^{3}He. It is therefore tempting to apply the standard Abrikosov-Gorkov (AG) model[29] of impurity scattering to the system. In this model, the order parameter is averaged over the impurities, and the scattering is homogeneous and isotropic. In such a model, the effect of the impurities is dominated by the size of the impurity limited mean free path l_{tr} relative to the coherence length ξ_0.[30] For ^{3}He in aerogel, l_{tr} would be equivalent to l_g, the geometrical mean free path that was described in Sec. II.

An early indication that a simple AG theory was insufficient to describe ^{3}He within aerogel was the relative robustness of T_c^a to the inclusion of impurities when compared to the suppression of ρ_s.[1,2,7] The disparity between the experimental results and the predictions[33] of the homogeneous scattering model can be seen in Fig. 10, where we have plotted the transition temperature suppression versus the low-temperature superfluid density. This robustness of T_c^a relative to ρ_s has also been seen in high-T_c superconductors and has

prompted extensions to the AG theory.[31] It has recently been pointed out by Franz *et al.*[31] that even for random impurities the AG formalism must break down for short coherence length superfluids, and in addition the width of the spatial distribution of the impurities must be taken into account. They argue that even for strongly scattering impurities the transition temperature will not be greatly affected as long as the scattering sites are spaced farther apart than the temperature-dependent coherence length $\xi(T)$. The temperature T_i, at which the coherence length is roughly equal to the impurity spacing $\xi(T_i) \simeq l_i$, should be the *lower bound* for the true T_c in the system. If the temperature predicted by the AG homogeneous scattering model, T_c^{AG}, is near or less than T_i, then the applicability of the AG theory is ''probably not justified.''[31]

We estimate the average impurity ''spacing'' l_i for cell C from the model to be twice the average value of the distribution of closest silica x in Fig. 4, which yields $l_i \simeq 200$ Å. At low pressure, where $\xi(T)$ is larger than l_i at all temperatures, the AG scattering model is more likely to be justified. At higher pressure, however, we estimate T_i/T_{c0} to be as large as 0.75 for $l_i = 200$ Å. (Here we have used Einzel's expression for the gap[32] at a pressure of 30 bar.) If we assume that the transport mean free path l_{tr} is roughly 2000 Å, the estimate for T_c^{AG}/T_{c0} from the homogeneous scattering model is approximately 0.75 at 30 bar.[7] The two temperatures T_i and T_c^{AG} are nearly the same, which calls into question the use of the AG model. We note that we have only assumed an average spacing of impurities. The consequence of variations in aerogel density that extend up to ξ_a, a length scale which is larger than the superfluid coherence length ξ_0, can only further restrict the applicability of the homogeneous scattering model. At high pressure we therefore expect the homogeneous scattering model to fail on two counts. First, the local impurity spacing does not allow the use of the homogeneous scattering model, even if the impurities were homogeneously distributed. Second, the variations in impurity density which extend up to ξ_a cannot be accounted for in the simple homogeneous scattering model.

Our reasoning for the inapplicability of the AG model is borne out by recent calculations,[7] which show that the AG model cannot describe the T_c suppression of superfluid ^{3}He, but that a model which includes strong inhomogeneity of scattering provides a much better description of the system. Neither sample is well described by the homogeneous model, but since the inhomogeneities in sample A are correlated over larger length scales, sample A is likely to be farther from the homogeneous regime than sample C. The average distance l_i is different from the correlation length ξ_a, but it should be related to ξ_a and the fractal correlations described by K_f. Although we do not have a model for the structure of sample A from which we can extract l_i, we expect that since sample A has a larger ξ_a and K_f, the average impurity spacing would also be larger than sample C. These length scales for cell A are consistent with the differences between the two samples shown in Fig. 10, and it explains why the T_c, ρ_s suppression in sample C is closer to the AG prediction.

The potential for the applicability of the homogeneous scattering model at low pressure is illustrated in Fig. 11, where we have plotted a two-dimensional cross section of the average local aerogel density $\overline{\rho_a}(\xi_0)$ for the model aerogel shown in Fig. 2(a). The figures were constructed starting from the same aerogel by averaging the local silica density over two different length scales, corresponding to the extreme values of ξ_0 realized in ^{3}He. The cross sections of the density plotted in Fig. 11 were calculated in the same plane as the slice shown in Fig. 3(a). Clearly, on the length scale appropriate at high pressure, the aerogel is rather inhomogeneous. At low pressure, the aerogel density averaged over the coherence length is almost constant.

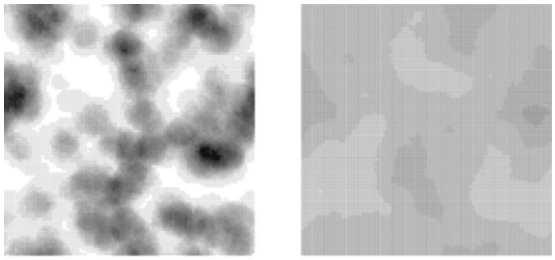

(a) (b)

FIG. 11. Two-dimensional cross sections of the local average aerogel density $\overline{\rho}(\xi)$ for the simulated aerogel shown in Fig. 2(a). The two figures represent *identical* aerogels, but the local density has been averaged over spheres of different sizes. The density in (a) was averaged over 200 Å, while in (b) it was averaged over 750 Å. The slice through the aerogel for both figures was taken at the same height as the slice shown in Fig. 3(a).

C. Scaling

Most of the scaled observables of bulk superfluid ^{3}He, such as the superfluid fraction ρ_s/ρ and heat capacity relative to the normal fluid C/C_N are predominantly functions of the ratio of the energy gap to the temperature Δ/k_BT. These observables also depend on Fermi-liquid corrections, and to a lesser extent, strong-coupling effects. For example, the superfluid density is given in the weak-coupling limit by[34]

$$\frac{\rho_s}{\rho} = \frac{1 - Y(\Delta/k_BT)}{1 + \frac{1}{3}F_1^s Y(\Delta/k_BT)}, \tag{2}$$

where $Y(x)$ is the Yosida function and F_1^s is the first symmetric Fermi-liquid parameter. In the weak-coupling limit, the behavior of $\Delta(T/T_c)$ is constrained and the scale for Δ is set by T_c. At pressures above 5 bar, F_1^s is not strongly pressure dependent and ρ_s/ρ is therefore a function of just T/T_c. One can see this scaling in Fig. 12, where we have plotted the bulk superfluid fraction at several pressures[24] as a function of T/T_c. The scaling is not perfect, of course, due to the Fermi-liquid corrections and strong-coupling effects. It is still true, though, that for weakly or strongly coupled BCS superfluids, the energy scale for pairing is set by T_c.[35]

The scaling with temperature of superfluid ^{3}He in aerogel contrasts sharply with the bulk behavior. We find that the superfluid fraction is a function of the *proximity* to the transition temperature, $\rho_s/\rho = f(T_c^a - T)$. Here the temperature is *not* scaled by T_c^{bulk} or T_c^a, and the only relevant energy scale appears to be $(T_c^a - T)$. The superfluid fraction measured in cell A is plotted as a function of $(T_c^a - T)$ in Fig. 13. At low

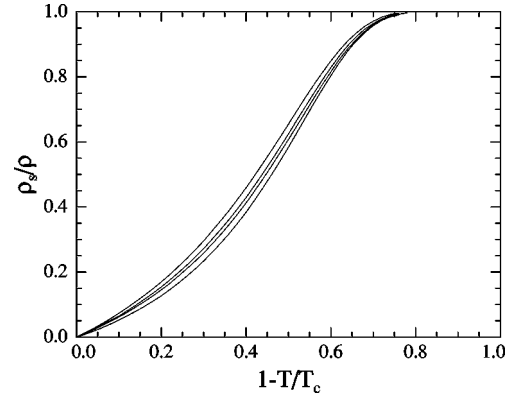

FIG. 12. The bulk superfluid fraction as a function of T/T_c, at pressures (from left to right) of 5, 10, 15, and 20 bar.

temperatures the superfluid density saturates at a limiting value which is strongly pressure dependent. It is clear, however, that the plots all have very nearly the same form between T_c^a and the pressure dependent saturation at low temperature. This behavior holds above 5 bar, and the collapse of the data at different pressures onto each other is extremely good if we group measurements above and below 15 bar separately. It is remarkable that this scaling behavior extends over such a large range in temperature and pressure. It appears that the pressure dependent microscopic properties of ^{3}He determine T_c^a and the low-temperature limiting value of the superfluid density, but between these points, the superfluid fraction is given by $\rho_s/\rho = f(T_c^a - T)$ where f is independent of pressure (and therefore ξ_0).

This scaling can also be seen in cell B (Fig. 14), where we plot the period shift as a function of $(T_c^a - T)$. The period shift has been scaled by the normal-fluid density, so that in the absence of parasitic resonances, the plots would be proportional to the superfluid fraction. The data extend over a rather limited range of pressure (11.4 to 29 bar), but the scaling observed for sample A is also apparent from these data. In both cases, the superfluid fraction at low pressure is too small to allow us to determine any change in the scaling of the superfluid fraction with temperature. We do not expect the same behavior to continue to low pressure, however,

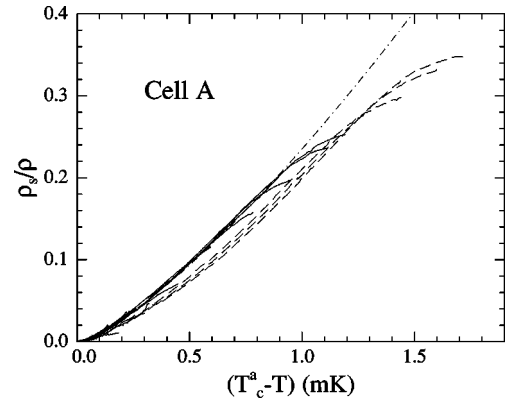

FIG. 13. ρ_s/ρ vs $(T_c^a - T)$ measured in cell A. The solid lines are measurements at 3.4, 3.9, 5.0, 6.1, 6.9, 8.5, 10.0, 12.9, and 15.0 bar. The dashed lines are measurements at 20.2, 25.0, and 29.0 bar. The dash-dotted line is a fit to a power law $\rho_s \propto (T_c^a - T)^n$ with $n = 1.33$.

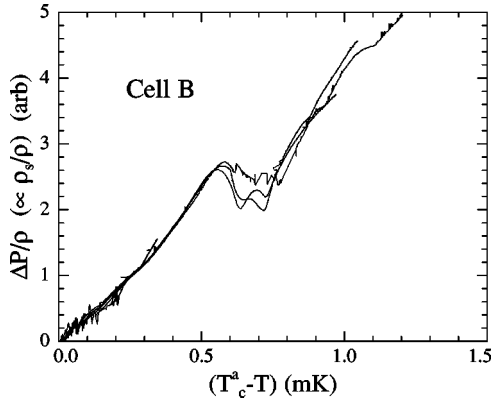

FIG. 14. The period shift divided by the bulk density $\Delta P/\rho$ plotted vs $(T_c^a - T)$ measured in cell B. The measurements were made at 11.5, 19.3, 21.5, 26.0, and 29.3 bar. The period shift due to the bulk fluid within the gap was subtracted as described in Sec. III (see Fig. 8).

based on low-temperature, low pressure measurements[3] on the similar aerogel of sample C. Providing the criteria for homogeneous scattering can be met, it is likely that at low pressures, the development with temperature of the superfluid fraction should exhibit a dependence similar to that predicted by the AG model. This behavior is discussed in the next section.

A natural question that arises is the effect of the nonhomogeneous distribution of the aerogel and its resultant tortuosity. We paraphrase the argument presented in Ref. 28. Unlike most other porous media, almost all of the aerogel structure is roughly the same size as the coherence length. For the tortuosity to be appropriately used, it has to describe the tortuous streamlines of a homogeneous superfluid. As a consequence, the scale of the structure of the porous medium has to exceed that of the superfluid ξ_0. All smaller scale structure is then manifested as intrinsic to the properties of the superfluid in the aerogel. This then leads to a ''coarse grained'' superfluid density.[36] At low pressure, where ξ_0 is large, this definition should pose no problems. Even at moderate pressure (20 bar) where the coherence length is $\sim$200 Å, tortuosity can only arise from structure greater than about 1000 Å in length scale, which approximately corresponds to the length scale where the structure appears homogeneous. Thus it is possible that there is a contribution to the tortuosity which may vary slightly with pressure (especially at high pressure), but because of the homogeneity of the aerogel at this length scale it is more appropriate to designate the tortuosity as approximately zero. Closer to T_c, where the coherence length is enhanced, the above arguments are further strengthened.

D. Temperature dependence of ρ_s

The temperature dependence of the development of the superfluid near T_c^a is also different from that of bulk ^{3}He. As with all BCS superfluids, the bulk superfluid density is linear with temperature very near T_c, since the BCS transition is well described by mean-field theory.[35] The linear behavior of $\rho_s(T)/\rho$ for the bulk fluid is limited to a fairly narrow region near T_c, as is shown in Fig. 15. One result of the AG model is that the presence of a homogeneous distribution of impu-

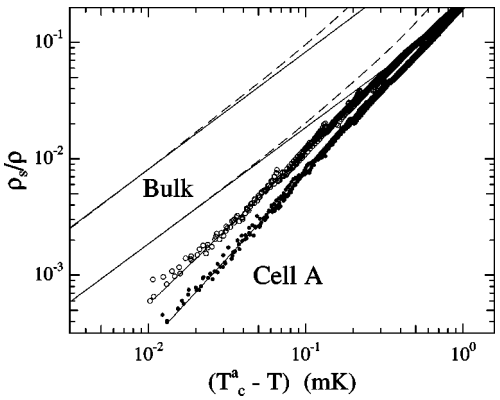

FIG. 15. A plot of $\log \rho_s/\rho$ vs $\log(T_c^a - T)$ measured in cell A. The open circles are measurements at 3.4, 3.9, 5.0, 6.1, 6.9, 8.5, 10.0, 12.9, and 15.0 bar. The solid circles are measurements at 20.2, 25.0, and 29.0 bar.

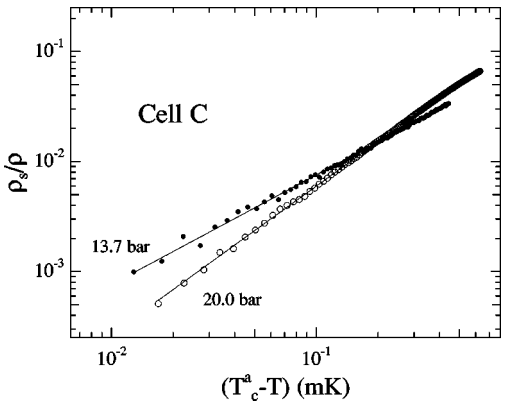

FIG. 17. A plot of $\log \rho_s/\rho$ vs $\log(T_c^a - T)$ measured in cell C. The solid circles are from a measurement made at 20.0 bar, and the open circles are from a measurement made at 13.7 bar.

rities should not modify the linear development of the superfluid fraction[7] observed for pure ^{3}He. In contrast, we find that the development of the superfluid density in aerogel is *not* linear with temperature, and the power-law dependence of $\rho_s(T)$ extends over a wide range of temperatures. This behavior indicates a qualitative as well as quantitative failure of the application of the AG model to this system.

Figure 15 shows $\log \rho_s/\rho$ at several pressures for cell A as a function of $\log(T_c^a - T)$. None of the curves show linear behavior, but instead exhibit a power-law dependence with an exponent n clearly larger than unity. At pressures below 5 bar it was impossible to accurately determine a power-law exponent. (At these low pressures the superfluid density was very small, and sound resonances[1] dominate the period shift at low pressures.) The exponents n (Fig. 16) vary between 1.45 and 1.3, and there is a distinct difference between the exponents above and below 15 bar ($\xi_0 = 245$ Å). The inhomogeneous scattering regime should give way to a homogeneous regime as the pressure is lowered (see Fig. 11). To illustrate this, we plot the measured exponents against the coherence length, ξ_0 normalized to ξ_a, the length scale at which the aerogel appears homogeneous (see Fig. 1). The lower pressure data from cell A exhibit behavior which is closer to linear, as we would expect from the arguments

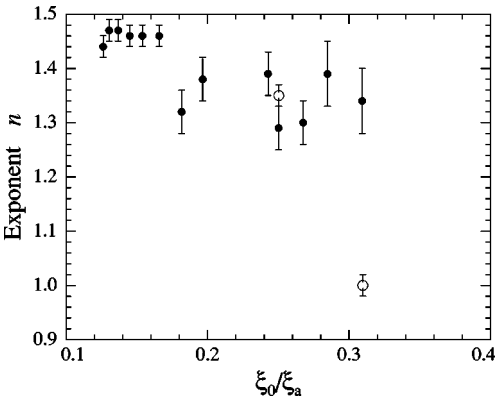

FIG. 16. The superfluid fraction power law n determined for cell A (solid circles) and C (open circles) as a function of the coherence length ξ_0 normalized to ξ_a, the length at which the aerogel appears homogeneous: $\rho_s(T)/\rho \propto (T_c^a - T)^{n(\xi_0/\xi_a)}$.

above. We note that the trend of a smaller exponent at lower ^{3}He density is different from the results obtained at Manchester[5] but we can offer no explanation for the discrepancy.

The resonances in the data from cell B make the determination of any power law for ρ_s/ρ impossible, but we can separate and thus subtract the bulk contribution to cell C with precision. The resulting ρ_s/ρ is shown in Fig. 17 at 13.7 and 20.0 bar, and the corresponding exponents are shown in Fig. 16. Remarkably, the superfluid in cell C has a greater than linear power-law dependence at 20 bar, but it is quite linear at 13.7 bar, once again exhibiting the power law over a large temperature range. The pressure dependence is consistent with our expectation since, of all the data, sample C at low pressure is most likely to be closer to the homogeneously scattering regime. Clearly, a systematic investigation of the power-law dependence on coherence length in the absence of a significant bulk fluid component is needed in order to compare details of the crossover of the superfluid behavior from the strongly inhomogeneous to the nearly homogeneous regime to theoretical expectations.

The change in power law away from the linear behavior near T_c as the pressure is increased is consistent with the behavior predicted for an inhomogeneous scattering model constructed by Thuneberg, Sauls, and co-workers.[7,37] By averaging the superfluid over the inhomogeneities they obtain nonlinear development of the superfluid near T_c at high pressures where the coherence length is small. As the pressure is lowered, the temperature development should crossover to a more linear behavior. It will be interesting to study superfluid ^{3}He in more dilute aerogels where the scale of the structure is different and so should exhibit behavior which deviates even further from a linear temperature dependence.

V. CONCLUSIONS

We have demonstrated that the structural correlations within aerogels play an essential role in determining the behavior of superfluid ^{3}He contained within them. The scattering data that we have obtained from samples used to measure both T_c^a and ρ_s/ρ emphasize that the volume fraction of the aerogel is only the starting point from which the superfluid behavior can be understood. Specifically, we have shown

that the aerogel can act as a nearly homogeneous or as a highly inhomogeneous impurity for identical density aerogels, depending on the size of the aerogel correlation length ξ_a relative to the superfluid coherence length ξ_0. Since the transport mean free path l_{tr} determines T_c^a in the homogeneous limit, while the aerogel correlation length ξ_a determines whether or not the system is actually homogeneous when compared to ξ_0, it would be very useful to vary these length scales independently. As we have discussed, this can be achieved by changing the pH of the aerogel growth environment, or by using different volume fraction aerogels grown in the base catalyzed regime. While we have shown that there is an evolution of the power-law behavior with pressure, this behavior has to be quantified further. It will likely prove to be important to obtain data from which the power law can be evaluated at low pressure and with different volume fractions of aerogel. The prospect of altering the fractal correlations in the growth process—thus changing K_f—holds forth the exciting possibility of quantifying the nature of the disorder and its effect on phase transitions.

ACKNOWLEDGMENTS

The authors would like to thank numerous individuals for their involvement during various parts of this project. Specifically we would like to recognize the contributions of K. Matsumoto, A. Golov, E. N. Smith, L. Pollack, R. Biggar, G. Lawes, J. Reppy, and C. Henley at Cornell. We also thank J. Yoon and N. Mulders who provided us with the aerogel samples which were grown at Penn State in M. H. W. Chan's lab. We also wish to thank M. Chan, W. P. Halperin, J. Sauls, E. Thuneberg, J. Hook, T. L. Ho, D. Einzel, and D. Sprague for discussions during various parts of this project. This research was supported by NSF Grant Nos. DMR-9424137 and DMR 97-05295, and a travel grant from NATO CRG-960127. Work at CHESS was supported under Grant No. NESF-DMR97-13424.

*Present address: National Institute of Standards, Gaithersburg, MD.

[1] J. V. Porto and J. M. Parpia, Phys. Rev. Lett. **74**, 4667 (1995).
[2] D. T. Sprague, T. M. Haard, J. B. Kycia, M. R. Rand, Y. Lee, P. J. Hamot, and W. P. Halperin, Phys. Rev. Lett. **75**, 661 (1995).
[3] K. Matsumoto, J. V. Porto, L. Pollack, T. L. Ho, and J. M. Parpia, Phys. Rev. Lett. **79**, 253 (1997).
[4] D. T. Sprague, T. M. Haard, J. B. Kycia, M. R. Rand, Y. Lee, P. J. Hamot, and W. P. Halperin, Phys. Rev. Lett. **77**, 4568 (1996).
[5] H. Alles, J. J. Kaplinsky, P. S. Wootton, J. D. Reppy, and J. R. Hook, Physica B **255**, 1 (1998).
[6] B. I. Barker, L. Polukhina, J. F. Poco, L. W. Hrubesh, and D. D. Osheroff, J. Low Temp. Phys. **113** (5/6), 635 (1998).
[7] E. V. Thuneberg, S. K. Yip, M. Fogelstrom, and J. A. Sauls, Phys. Rev. Lett. **80**, 2861 (1998).
[8] G. E. Volovik, Pis'ma Zh. Éksp. Teor. Fiz. **63**, 281 (1996) [JETP Lett. **63**, 301 (1996)].
[9] V. P. Mineev, Pis'ma Zh. Éksp. Teor. Fiz. **66**, 655 (1997) [JETP Lett. **66**, 693 (1997)].
[10] *Proceedings of the Fourth International Symposium on Aerogels*, edited by R. W. Pekala and L. W. Hrubesh [J. Non-Cryst. Solids **186** (1995)].
[11] R. Vacher, T. Woignier, J. Pelous, and E. Courtens, Phys. Rev. B **37**, 6500 (1988).
[12] D. W. Schaefer and K. D. Keefer, Phys. Rev. Lett. **56**, 2199 (1986).
[13] A. Hasmy, R. Vacher, and R. Jullien, Phys. Rev. B **50**, 1305 (1994).
[14] The aerogel samples were grown for us by N. Mulders and J. Yoon in M. H. W. Chan's laboratory at the Penn. State University. The aerogels were grown under basic conditions as described in T. M. Tillotson and L. W. Hrubesh, J. Non-Cryst. Solids **145**, 44 (1992).
[15] A. Hasmy, E. Anglaret, M. Foret, J. Pelous, and R. Jullien, Phys. Rev. B **50**, 6006 (1994).
[16] E. Anglaret, A. Hasmy, and R. Jullien, Phys. Rev. Lett. **75**, 4059 (1995).
[17] R. Jullien and A. Hasmy, Phys. Rev. Lett. **74**, 4003 (1995).
[18] S. Brunauer, P. H. Emmett, and E. Teller, J. Am. Chem. Soc. **60**, 309 (1938).
[19] P. Meakin, J. Colloid Interface Sci. **102**, 491 (1984).
[20] A. Hasmy, M. Foret, J. Pelous, and R. Jullien, Phys. Rev. B **48**, 9345 (1993).
[21] Alain Le Méhauté, *Fractal Geometries, Theory and Applications* (CRC Press, Boca Raton, 1991).
[22] T. Hall, S. M. Tholen, K. R. Lane, V. Kotsubo, and J. M. Parpia, J. Low Temp. Phys. **89**, 897 (1992).
[23] *Experimental Techniques in Condensed Matter Physics at Low Temperatures*, edited by R. C. Richardson and E. N. Smith (Addison-Wesley, Redwood City, 1988).
[24] J. M. Parpia, D. G. Wildes, J. Saunders, E. K. Zeise, J. D. Reppy, and R. C. Richardson, J. Low Temp. Phys. **61**, 337 (1985).
[25] D. Einzel and J. M. Parpia, Phys. Rev. Lett. **58**, 1937 (1987).
[26] D. S. Greywall, Phys. Rev. B **33**, 7520 (1986).
[27] The change in slope in the scattering data that signals the crossover to the surface regime actually occurs at a slightly larger length, ≈ 50 Å. This is to be expected for polydisperse particles,[13] since the surface scattering is dominated by the few largest particles. Fitting to the model aerogel, as opposed to determining the wavelength of the crossover $(2\pi/q)$, is a more accurate method for determining a. We can, however, use the locations of the changes in slope on the scattering plot to compare the length scales in samples A and C.
[28] A. Golov, J. V. Porto, and J. M. Parpia, Phys. Rev. Lett. **80**, 4486 (1998).
[29] A. A. Abrikosov and L. P. Gorkov, Zh. Éksp. Teor. Fiz. **39**, 1781 (1960) [Sov. Phys. JETP **12**, 1243 (1961)].
[30] The order parameter strength is also affected by the phase shifts at scattering which range between the weak (Born) to the strong (unitary) limits. However, T_c^a/T_{c0} is set by the ratio l_{tr} to ξ_0.
[31] M. Franz, C. Kallin, A. J. Berlinsky, and M. I. Salkola, Phys. Rev. B **56**, 7882 (1997).
[32] D. Einzel, J. Low Temp. Phys. **54**, 427 (1984).
[33] R. Hanninen, T. Setala, and E. V. Thuneberg, Physica B **255**, 11 (1998).
[34] J. W. Serene and D. Rainer, Phys. Rev. B **101**, 221 (1983).
[35] A. J. Leggett, Ann. Phys. (N.Y.) **85**, 11 (1974).
[36] P. A. Crowell, J. D. Reppy, S. Mukherjee, J. Ma, M. H. W. Chan, and D. W. Schaefer, Phys. Rev. B **51**, 12 721 (1995).
[37] E. Thuneberg and J. Sauls (private communication).